IEEE Access
Multidisciplinary ⋮ Rapid Review ⋮ Open Access Journal

Received 8 February 2023, accepted 17 February 2023, date of publication 8 March 2023, date of current version 14 March 2023.

Digital Object Identifier 10.1109/ACCESS.2023.3254207

RESEARCH ARTICLE

Investigation Into the Effect of Joint Clearance on the Dynamics of a Biomechanical Energy Harvesting System

LUDWIN MOLINA ARIAS[1], MAREK IWANIEC[2], AND JOANNA IWANIEC[3]

[1]Department of Process Control, Faculty of Mechanical Engineering and Robotics, AGH University of Science and Technology, 30-059 Kraków, Poland
[2]Department of Biocybernetics and Biomedical Engineering, Faculty of Electrical Engineering, Automatics, Computer Science and Biomedical Engineering, AGH University of Science and Technology, 30-059 Kraków, Poland
[3]Department of Robotics and Mechatronics, Faculty of Mechanical Engineering and Robotics, AGH University of Science and Technology, 30-059 Kraków, Poland

Corresponding author: Ludwin Molina Arias (arias@agh.edu.pl)

This work was supported in part by the Program Excellence Initiative-Research University for the AGH University of Science and Technology; and in part by the INNOGLOBO/InnoIndie Project: "System for monitoring the conditions of transport of sensitive materials, including food and hazardous materials."

ABSTRACT The existing clearance in the mechanical joints plays a crucial role in the assembly of mechanical systems, allowing the mobility of its components. However, few studies have explored models that consider joint clearance in the case of electromechanical energy harvesting systems. This paper examines the effect of existing clearance in an electromagnetic energy harvester attached to the human lower limb. The dynamic response of the system and an estimate of its generated power are obtained by developing a lumped model, in which clearance is included by adding a dead band and assigning a stiffness coefficient during contact between elements. The natural motion of the lower limb is the input to the formulated model, which takes into account the nonlinear interaction of the electromagnetic device and the power conditioning circuit. Central composite design is used to study the influence of two selected factors on the dynamics of the system; joint clearance size and contact stiffness. The results suggest that the presence of clearance between the clamping mechanism and the human body positively affects the performance of the analyzed electromagnetic energy harvesting system. It was revealed that an increase of around 27% of output power could be intentionally achieved by adding larger clearance sizes.

INDEX TERMS Biomechanics, electromagnetic induction, electromechanical system modeling, energy harvesting, joint clearance.

I. INTRODUCTION

Ranging from phones, watches, and health monitoring devices to prostheses and exoskeletons, wearable electronic devices have improved the quality of human life by changing the way information is transmitted and received. As the performance of electronic devices continues to increase while shrinking in size, interest in alternative and portable power sources has grown significantly in recent years.

The associate editor coordinating the review of this manuscript and approving it for publication was Youngjin Kim.

Extensive research has been carried out and many devices have been developed with the aim of harvesting energy from human movement and effectively meeting the energy demand for small power devices [1], [2]. The operating principle of a biomechanical energy harvester consists of the usage of energy conversion devices, based mainly on electromagnetic, electrostatic, piezoelectric, and triboelectric effects, to transform kinetic energy into useful electrical energy [3], [4], [5]. Among the different body movements considered for energy harvesting, most of the research has focused on the linear movement of the center of mass and the rotational movement of human joints, such as the shoulders, wrists, knee,

ankle, and hip joint [6], [7], [8]. In all these cases, the main challenge in designing a biomechanical energy harvester is to build devices that work efficiently, but interfere as little as possible with the natural processes of the body [9]. A small amount of harvested energy might not be enough to power electronics, and an excessive amount can cause over-effort of the user. To address this problem, researchers have focused on harvesting energy from unwanted phenomena, such as vibrations caused by the interaction of the human body with its environment [10], [11], [12] and physical activities in which muscles perform negative mechanical work. Donelan et al. [13] designed a device capable of assisting the muscles of the human lower limb, while harvesting energy. The electromagnetic device is attached to the knee joint and works only when the muscles naturally take over energy absorption. Similarly, Collins and Kuo [14] followed the same approach and designed a prosthetic foot to capture energy from heel strike and reduce user effort in liftoff. The constructed device consists of mechanical springs that can engage and disengage depending on the moment within the gait cycle.

Regardless of the phenomenon associated with the operating principle of the energy conversion device, mechanical systems must be used to attach the device to the human body. The mechanical system that interacts with the human body commonly consists of flexible elements that not only ensure the correct positioning of the device, but also guarantee the comfort of the user. In the literature, two different approaches are followed to analyze the performance of the entire system. The first and most widely used approach consists of building a prototype and performing experiments [15], [16]. The second approach consists of making consistent assumptions, obtaining the mathematical model of the system, and performing numerical simulations to calculate the variables of interest [17]. In the case of following modeling approach, the analysis of mechanical systems is commonly carried out considering perfect kinematic constraints between the components, thus neglecting the presence of joint clearances.

In practice, the presence of clearance between mechanical components is inevitable and necessary for the correct assembly and mobility of the system. Unfortunately, it is well known that even small looseness in the joints of mechanical components generate impact forces that significantly increase dynamic stress [18], reduce the precision of movements [19], and can lead to chaotic behavior [20]. Despite the interest in developing alternative energy sources for portable devices, few studies have considered gaps in energy harvesting systems [21]. Consequently, there is a great need to investigate the influence of nonlinearities produced by the presence of clearance on the dynamics of energy conversion devices, seeking the development of more efficient biomechanical energy harvesting systems.

The main contributions of this paper are as follows: (1) formulation of a dynamic model to estimate the response of a biomechanical energy harvesting system in the presence of clearance between the energy conversion device and the human body, and (2) application of sensitivity analysis to explore the influence of clearance on the dynamics and efficiency of biomechanical energy harvesters.

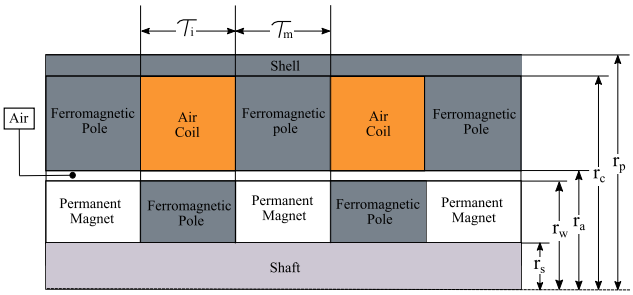

FIGURE 1. Transverse view of the electromagnetic induction-based device.

II. ELECTROMAGNETIC INDUCTION-BASED DEVICE

The main component of an electromagnetic energy harvesting system (EEHS) is an electromagnetic induction-based device (EID). Fig. 1 shows the transverse view of the EID under study. The function of the device is to transform the kinetic energy associated with the movement of the knee joint into electrical energy by exploiting electromagnetic induction. The EID considered in this study has a tubular shape and consists of a set of permanent magnets that move inside a set of air coils. Magnets and coils are separated by ferromagnetic rings and covered by a ferromagnetic case, which facilitates and directs the magnetic flux from the magnets radially towards the coils. The ends of the EID are attached to the human thigh and shank using flexible clamps. The device shaft, accompanied by the set of magnets, moves linearly as a result of the natural rotation of the knee joint, changing the magnetic flux that travels across the surface of the air coils. An electromotive force (EMF) is induced between the terminals of the set of coils according to the Faraday law of induction:

$$EMF = -\frac{\partial B}{\partial x}\frac{dx}{dt} = -K_v(x)\frac{dx}{dt} \tag{1}$$

where B is the magnetic field induction, x is the linear displacement, t is the time, and K_v is the back EMF constant.

The magnitude of the induced EMF is proportional to the velocity of the excitation movement, and its frequency depends on the dimensions of the EID components and the way in which they are arranged within the device. The value of the back EMF constant can be estimated using analytical, numerical, or experimental approaches. In this study, the methodology suggested in [22] has been followed for its estimation. This methodology employs a lumped equivalent magnetic circuit, which makes the simplified assumption that the magnetic resistance of each component is concentrated on idealized electrical resistors linked by a network of perfectly conducting wires. Following this methodology, the amplitude and frequency of $K_v(x)$ are calculated knowing the dimensions and materials of the components of the EID.

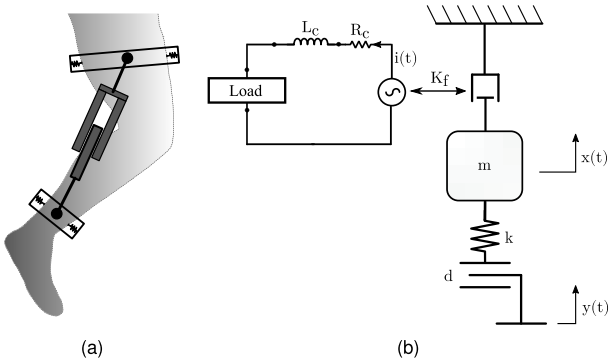

FIGURE 2. (a) Schematic view of the device attached to the lower limb. (b) Schematic model of the system.

III. JOINT CLEARANCE MODELING

The presence of clearance in the joints of mechanical systems is an inevitable fact. In this study, the EEHS model is derived considering the existing clearance within the joint that holds the device to the lower limb. Fig. 2 shows the scheme of the model considered.

As a result of the existing joint clearance, small collisions occur between the clamp that holds the device to the human body and the human body itself. The resulting motion can be considered as the superposition of kinematic excitation (natural movement of the knee joint) and small vibrations, the frequency of which is determined by the natural frequency of the whole system. The combined movement drives the EID, which transforms the excitation (movement) into useful energy, but also the induced vibrations. The equation of motion of the system under consideration is obtained by applying Newton's second law along the vertical axis of the scheme shown in Fig. 2. The restoring force added by the presence of joint clearance has been modeled using a linear function with a deadband weighted by a coefficient that considers the stiffness of the elements involved in the collisions [23]. The stiffness coefficient considered corresponds mainly to the stiffness of human tissues and the clamps used to fasten the energy conversion device to the human body. In (2), the mathematical expression that models the considered mechanical system is presented:

$$m\ddot{x} + c\dot{x} + k_d U(x, y) = 0 \tag{2}$$

where m is the mass of the upper moving component, which includes the EID slider and the upper clamp, k_d is the stiffness of the elements involved during collisions, which we refer to as contact stiffness. x is the resulting displacement, y is the excitation movement, c is the mechanical damping produced by the electromagnetic device, and $U(x, y)$ is a nonlinear function, which varies according to (3).

$$U(x, y) = \begin{cases} x(t) - y(t) + d, & x(t) - y(t) > d, \\ 0, & -d < x(t) - y(t) < d \\ x(t) - y(t) - d, & x(t) - y(t) < -d \end{cases} \tag{3}$$

where d is the clearance size.

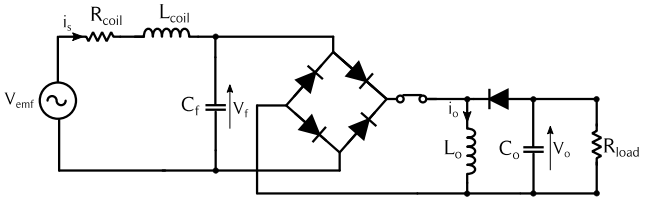

FIGURE 3. Electronic circuit representing the energy harvesting device connected to the power conditioning circuit.

Since electric current, voltage, and damping force are variables that depend on the form of connection between the coils and the external load, the model must take into account the interaction between the energy conversion device and the power conditioning circuit employed [24]. In this work, the EID is connected to an AC-DC rectifier followed by a step-up and step-down converter that adjusts the output voltage level to the required value.

The electronic circuit representing the entire EEHS under study is shown in Fig. 3. It comprises an EID, an AC-DC rectifier, a buck-boost converter, and an external load. The EID is represented as an AC voltage source connected in series to a coil and a resistor, representing the internal inductance and the electric resistance of the EID, respectively. The rectifier is made up of a full-bridge rectifier and a capacitor. The buck-boost converter is a DC-DC converter that varies the voltage level at the output according to the duty cycle of a PWM signal responsible for setting the state of a switch. Assuming that the switching frequency is sufficiently high, Kirchhoff's laws can be applied to obtain the state-space averaging equations [25]. The state-space averaging approach computes the global effect of one period by weighting the contribution of each stage of the switching converter. Therefore, average currents and voltages are used to describe the behavior of the circuit.

$$\frac{di_s}{dt} = -\frac{R_{coil}}{L_{coil}} i_s - \frac{1}{L_{coil}} V_f + \frac{1}{L_{coil}} V_{emf} \tag{4}$$

$$\frac{dV_f}{dt} = \frac{1}{C_f} i_s - D\frac{sign(V_f)}{C_f} i_o \tag{5}$$

$$\frac{di_o}{dt} = D\frac{sign(V_f)}{L_o} V_f + (1 - D)\frac{\lambda}{L_o} V_o \tag{6}$$

$$\frac{dV_o}{dt} = -(1 - D)\frac{\lambda}{C_o} i_o - \frac{1}{R_{coil} C_o} V_o \tag{7}$$

where R_{coil} is the internal coil resistance, L_{coil} is the internal coil inductance, C_f is the rectifier capacitance, L_0 is the inductance of the buck boost converter, C_o is the capacitance of the buck boost converter, R_{load} is the load resistance, D is the duty cycle of the PWM switching signal, and λ is a binary term, the value of which depends on the state of the diode according to the expression (8).

$$\lambda = \begin{cases} 1, & i_0 \geq 0 \\ 0, & i_0 < 0 \end{cases} \tag{8}$$

TABLE 1. Dimensions and magnetic properties of the electromagnetic device components.

Symbol	Description	Value
τ_m	Magnet height	10 mm
r_s	Shaft radius	3 mm
$r_w - r_s$	Magnet width	8 mm
$r_a - r_w$	Air Gap	1.5 mm
τ_i	Tooth height	10 mm
$r_c - r_a$	Coil width	9.5 mm
$r_p - r_c$	Stator shell thickness	3 mm
d_z	Coil wire diameter	0.4 mm
B_{rem}	Remanent magnetic flux density	1.23 T
N	Turn coil	593
nC	Number of coils	5
μ_0	Air / Cooper relative permeability	1
μ_{Fe}	PLA relative permeability	4

where i_0 is the electric current flowing through the converter coil.

The mathematical model obtained consists of a second-order nonlinear differential equation that models the system in the mechanical domain (3) and four first-order differential equations that model the system in the electrical domain (4)−(7). To obtain the solution of the set of differential equations, numerical methods have been used.

IV. SIMULATION SETUP AND PRELIMINARY RESULTS

The dimensions of the EID were selected considering that it would be robust enough to produce significant electrical energy, but without adding an excessive load on the user. Harmonic kinematic excitation with an amplitude equal to 500 mm and a frequency of 0.8 *Hz* was assumed. These values were selected taking into account walking on flat ground under normal conditions. A preliminary joint clearance size of 5 mm, a contact stiffness of 50 kN/m, a load resistance of 750 Ω, and a device mass of 2 *Kg* were assumed. All ferromagnetic components are made of magnetic iron PLA, which is a compound of PLA and finely ground iron powder that can be used in 3D printing. The rest of the components are air coils made of cooper and neodymium magnets. The dimensions and relevant properties of the EID components are presented in Table 1.

The parameters of the electronic circuit are presented in Table 2. These values were selected in order to ensure a semi-stable voltage output level and a short time to reach steady state. To define the value of internal inductance and resistance of the EID, the analytical expression found in [26] was used.

Using the selected values, the differential equations that describe the dynamics of the system were obtained, and they were solved by implementing the trapezoidal rule. This technique calculates two derivatives using Euler forward and backward steps and then averages them to obtain a more appropriate value with a smaller numerical error [27]. All numerical calculations were performed using MATLAB-written codes.

TABLE 2. Electronic parameter values of the electromagnetic induction-based device and the power conditioning circuit.

Symbol	Description	Value
R_{coil}	Internal coil resistance	42.7 Ω
L_{coil}	Internal coil inductance	286 mH
C_f	Rectifier capacitance	0.1 mF
L_o	Buck-boost converter inductance	50 mH
C_o	Buck-boost converter capacitance	8.5 mF

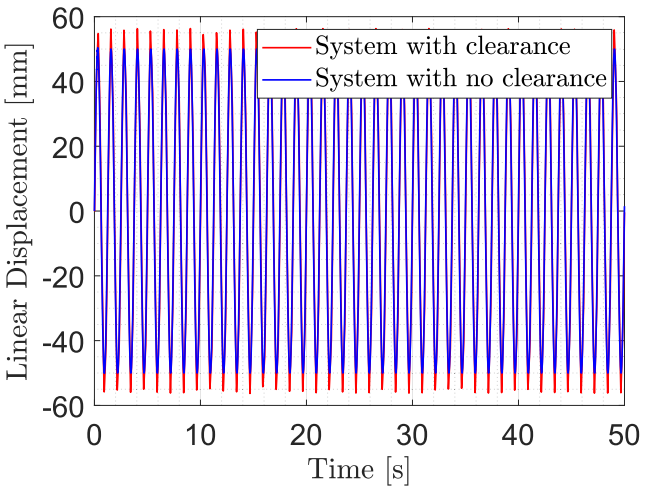

FIGURE 4. Linear displacement of the EID slider.

Fig. 4 shows the resulting mechanical displacement of the EID slider. The response of the system under harmonic excitation is also a harmonic response of the same frequency, but superimposed on small oscillations produced by the presence of joint clearance. It should be noticed that the proposed EEHS is capable of convert almost all the added oscillations into energy, and therefore the response obtained is almost identical to the excitation movement, differing only by a slight increase of the amplitude. Fig. 5 shows the useful voltage generated (voltage at the terminals of the external load). The output voltage has reverse polarity compared to the output voltage of the rectification stage. Once the transient state ends, a semi-stable behavior is observed, which oscillates around −11 V. It can be seen that the resulting signal consists of various harmonic functions of different frequencies, which, compared to the voltage generated in the absence of clearance, have a greater deviation from the mean value. Similarly, Fig. 6 shows the output power, which is the actual power consumed by the device connected to the energy harvesting system. It can be observed that the resulting output power, compared to the output power without joint clearance, contains lower frequencies of higher amplitude that produce a slight increase in the average power.

These results consider fixed parameters that were previously specified. To investigate the influence of the selected parameters on the results obtained, several simulations must be performed in which these parameters are varied.

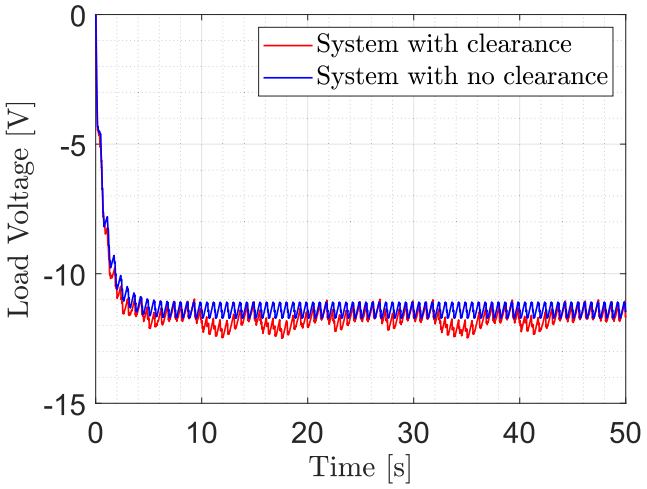

FIGURE 5. Voltage across the electric load.

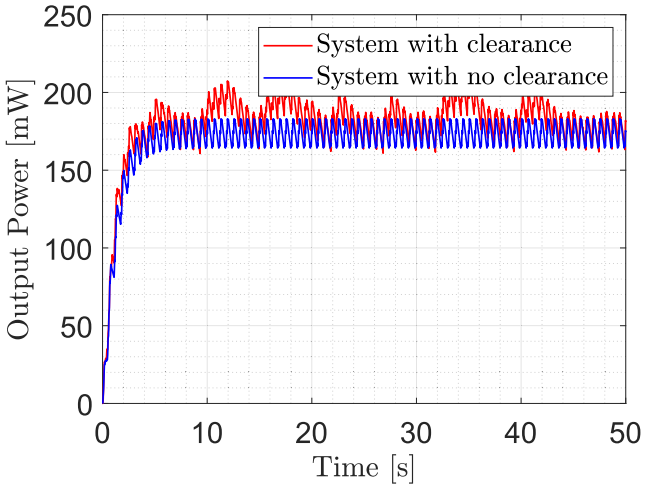

FIGURE 6. Power consumed by the electric load.

TABLE 3. Range of the selected factors.

Symbol	Description	Min	Max
d	Clearance	0 mm	10 mm
k_d	Contact Stiffness	0.5 kN/m	50 kN/m

V. RESPONSE SURFACE METHODOLOGY

Design of experiments (DoE) is used to investigate the effect of joint clearance on the dynamic response of the electromechanical system analyzed. This set of statistical procedures is used in several investigations to perform optimizations in device construction and to analyze the effect of selected variables in hypothetical scenarios [28], [29], [30]. Joint clearance size (d) and stiffness contact (k_d) are the dependent variables selected (factors) for evaluation, while power mean (P_{mean}), power standard deviation (P_{std}), power root mean square (P_{rms}), and the time it takes for the system to stabilize (t_{ss}) are the dependent variables. The limits established for the independent variables are presented in Table 3.

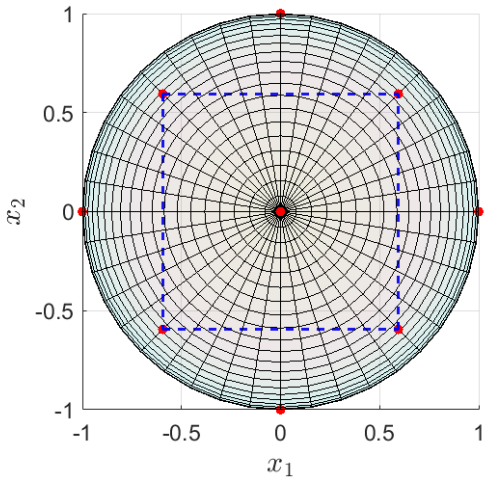

FIGURE 7. Three-dimensional space showing the combinations considered.

The selected experimental design corresponds to the central composite design (CCD), which belongs to the response surface methodology (RSM). The selection of CCD obeys the fact that it is possible to build a second-order model with fewer observations than in the case of a three-level factorial design. CCD is based on a two-level factorial design with the addition of a central point and $2k$ star points (k is the number of factors) between the axes, which allow us to model the curvature within the model. Within CCDs, three types can be used: Circumscribed, Inscribed, and Face-Centered. In this study, the inscribed CCD was used, since in its design the range of factors values does not exceed the limits imposed when planning the experiment.

Since two factors are considered in this study, nine combinations (observations) constitute the design matrix. Fig. 7 shows the distribution of the design matrix in a plane, where each axis corresponds to a given factor.

In Table 4 the design matrix is presented, in which the columns are divided into studied factors and dependent variables. On the side of the studied factors, the columns x_1 and x_2 correspond to the factors scaled in an interval of -1 to 1. The actual values are presented in the remaining column. On the side of dependent variables, the actual values of P_{mean}, P_{std}, P_{rms}, t_{ss} are presented. These values were computed using the factor values for each observation. Similarly to the earlier calculations, a harmonic kinematic excitation of amplitude equal to 500 mm and frequency equal to 0.8 Hz was assumed. The chosen sampling frequency was 10000 Hz, and the trapezoidal rule was used to solve the nonlinear differential equations.

The design matrix is used in the following subsections for an analysis of the dynamic behavior of the system when the factors are varied separately and simultaneously.

A. LOCAL SENSITIVITY CURVES

Fig. 8, and Fig. 9 were constructed by plotting the values of one factor against the corresponding output, while the

TABLE 4. Design matrix.

	Studied Factors				Dependent Variables			
No	x_1	x_2	d [mm]	k_d [kN/m]	P_{mean} [mW]	t_{ss} [s]	P_{std} [mW]	P_{rms} [mW]
1	-0.7071	-0.7071	1.400	7.749	276.374	10	15.734	276.819
2	-0.7071	0.7071	1.400	42.750	245.082	10	16.363	245.626
3	0.7071	-0.7071	8.500	7.749	279.933	10	9.745	280.101
4	0.7071	0.7071	8.500	42.750	262.703	10	12.645	263.005
5	-1	0	0.000	25.250	210.159	10	12.662	210.539
6	1	0	10.000	25.250	275.845	10	10.988	276.062
7	0	-1	5.000	0.500	496.685	10	30.278	497.602
8	0	1	5.000	50.000	276.380	10	15.939	276.837
9	0	0	5.000	25.250	277.542	55	15.104	277.950

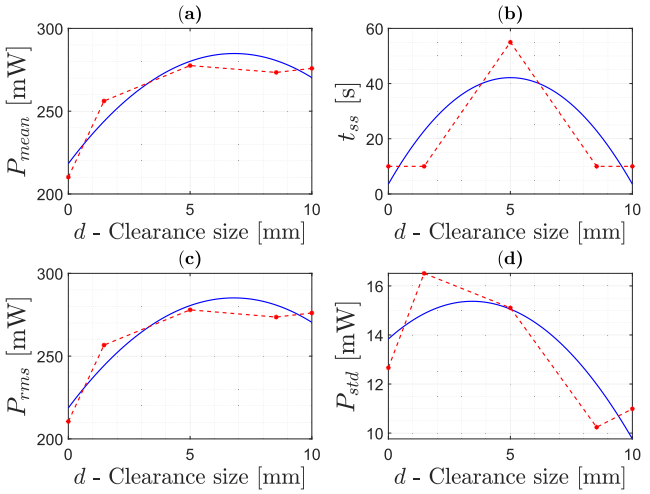

FIGURE 8. Local Sensitivity Curves for clearance size. (a) mean power, (b) time to reach steady state, (c) root mean square power, and (d) standard deviation power.

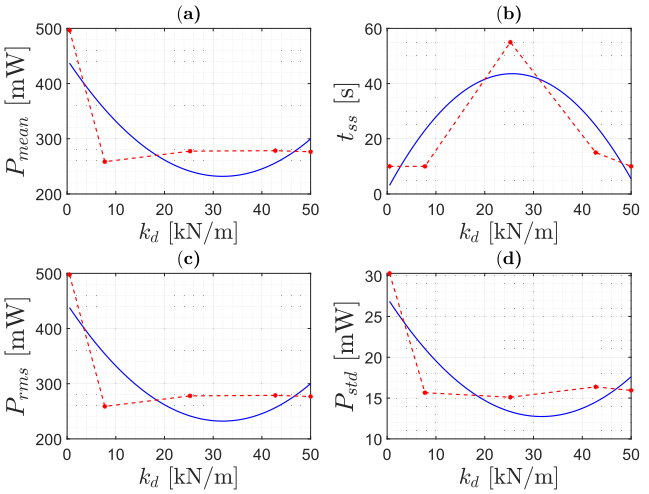

FIGURE 9. Local sensitivity curves for contact stiffness. (a) mean power, (b) time to reach steady state, (c) root mean square power, and (d) standard deviation power.

other factor remains constant at its central value. The plotted points, which represent the observation, were also connected with straight lines. The slopes of these lines are an indicator of the importance of each factor in the dependent variable considered. In the plots, a second-order approximation using least-squares regression is also presented.

Fig. 8 shows the sensitivity curves determined for the first factor, which corresponds to the clearance size. It was revealed that P_{mean} and P_{rms} increase with increasing d until it reaches a value of about 6 mm, which corresponds to 1.2% of the amplitude of the excitation motion. Once d is larger, the power output tends to be constant. Looking at Fig. 8(b), it can be seen that t_{ss} has a local maximum when d has a value around 5 mm. P_{std} tends to increase with increasing d, but decreases rapidly when considering high d values. Fig. 9 presents the sensitivity curves obtained when the contact stiffness is varied. In this case, t_{ss} is observed to have a behavior similar to that observed in the sensitivity curves corresponding to the clearance size. In contrast, P_{rms}, P_{mean}, and P_{std} decrease rapidly with increasing k_d, reaching a minimum value when the contact stiffness is around 30 kN/m.

The impact of the studied factors on the dependent variables was obtained by computing the derivative of the linear functions that constitute the local sensitivity curves. The derivatives were calculated by taking the difference between the minimum and maximum values of the dependent variable in the considered range and normalizing it using the difference between the minimum and maximum values of the corresponding factor within the same range. The sign of the obtained value specifies whether an increase in the corresponding factor increases (positive sign) or decreases (negative sign) the dependent variable studied. The results obtained are presented using bar charts, where each bar represents the relevance of the corresponding factor in each interval. Since the local sensitivity curves are made up of five points, four intervals have been considered.

Fig. 10 shows the impact of the studied factors on P_{mean}. The relationship between d and P_{mean} is observed to be directly proportional, with the exception of the 3^{rd} interval. However, since the impact has a value close to 0, it could be inferred that d has almost no effect on P_{mean} in this interval. It is also observed that the impact of d on power output decreases with increasing d. Similarly, looking at the impact of k_d on the power output, we notice that only in the 1^{st} interval, that is, at low values of k_d, there is a significant impact.

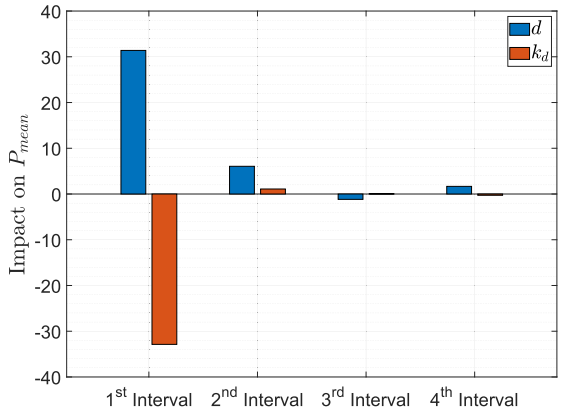

FIGURE 10. Impact of studied factors on P_{mean}.

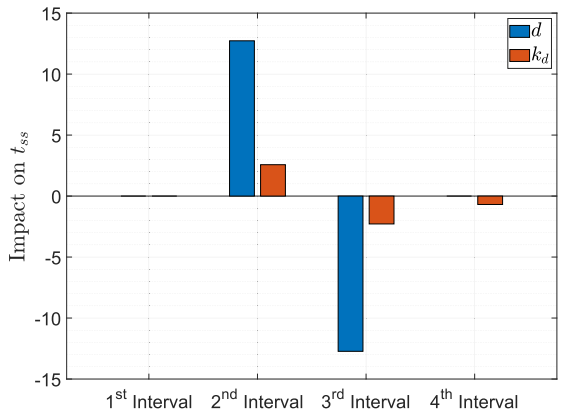

FIGURE 11. Impact of studied factors on t_{ss}.

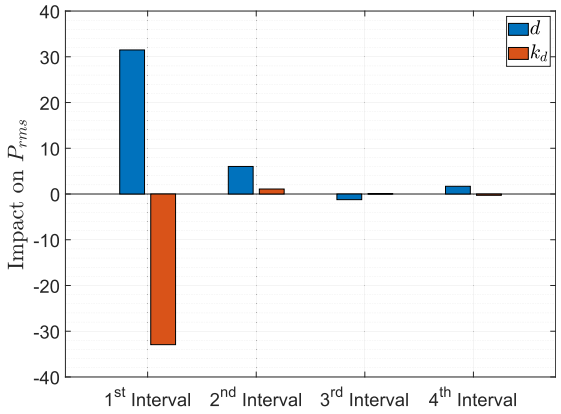

FIGURE 12. Impact of studied factors on P_{rms}.

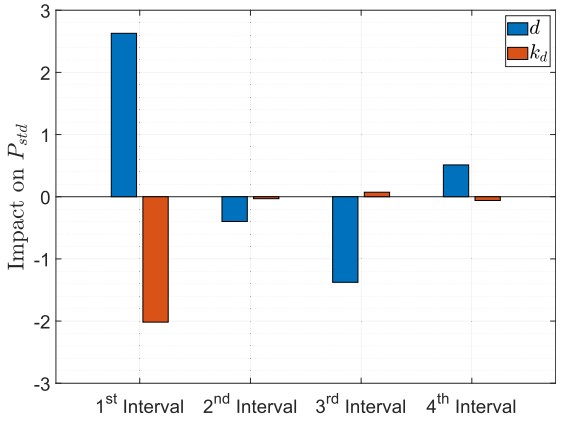

FIGURE 13. Impact of studied factors on P_{std}.

Fig. 11 shows the impact of the studied factors on t_{ss}. The relationship between t_{ss} and the factors studied is found to be insignificant in the 1^{st} interval. Then, there is a change of sign once the 3^{nd} interval is reached. This suggests that a critical point can be found between the 2^{nd} and 3^{rd} intervals.

The results presented in Fig. 12 have the same behavior as those presented in Fig. 10. This fact is explained because the sign of the power output is always positive, therefore the P_{rms} and the P_{mean} must be equal.

Fig. 13 shows the impact of the studied factors on P_{std}. Here, it is evident that varying d has significantly more impact on power output variability than varying k_d. Furthermore, although the impact of k_d on P_{std} is positive only on the 3^{rd} interval, the impact on the 2^{nd}, 3^{rd}, and 4^{th} interval is still small enough (compared to the highest value in the interval 1^{st}) to assume that k_d only has an impact on P_{std} in the 1^{st} interval.

The disadvantage of using local sensitivity curves is the inability to evaluate the interaction between several factors and the global impact on the system output. To overcome this issue, in the following subsections, the design matrix was used to estimate the response surface of the system under study.

B. RESPONSE SURFACE PLOTS

For each of the nine combinations of factors, a numerical experiment was carried out using MATLAB. Since the aim of the device is to collect as much energy as possible, P_{rms} is the dependent variable analyzed and presented in the response surface plots. Three different polynomials were selected to estimate the mathematical function that models the system, and the least squares approach was used to fit the data. The simplest approximation function used was a first-order polynomial, in which each factor has an associated proportionality constant. The second approximation function makes use of a proportionality constant for each factor and considers the interaction between each pair of factors by adding the multiplication of them weighted by a proportionality constant. The last approximation function used is a second-order polynomial. The corresponding mathematical expressions are presented below.

Model 1:

$$f(x_1, x_2) = b_0 + b_1 x_1 + b_2 x_2$$

Model 2:

$$f(x_1, x_2) = b_0 + b_1 x_1 + b_2 x_2 + b_3 x_1 x_2$$

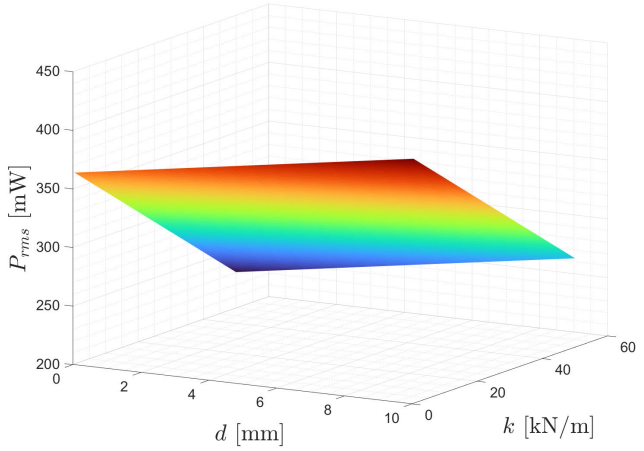

FIGURE 14. Response surface plot obtained using linear approximation.

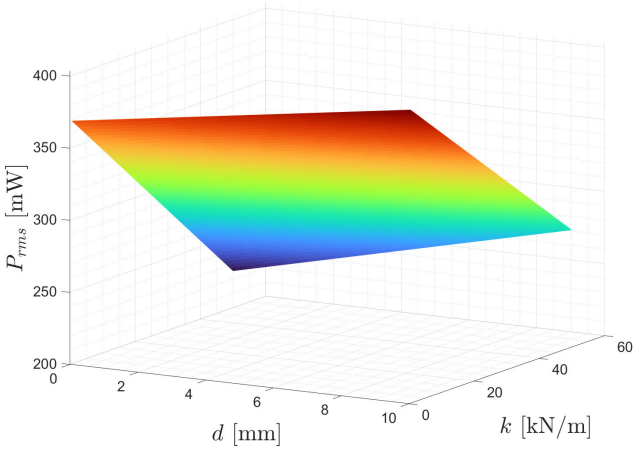

FIGURE 15. Response surface plot obtained using linear approximation considering factor interactions.

Model 3:

$$f(x_1, x_2) = b_0 + b_1x_1 + b_2x_2 + b_3{x_1}^2 + b_4{x_2}^2$$

where $f(x_1, x_2)$ is the value of the dependent variable (P_{rms}), and b_0, b_1, b_2, b_3 and b_4 are measures of the impact of the given combination of factors.

Fig. 14 shows the response surface plot obtained for the case where a first-order approximation is used to model the system (Model 1). The surface obtained is a perfect plane with a certain level of inclination with respect to both axes. Furthermore, it is evident that d is directly proportional to the output power, whereas k_d is inversely proportional.

Fig. 15 shows the response surface obtained for the case of a linear approximation considering also the interaction between each pair of factors (Model 2). Ideally, the surface obtained is not a perfect plane, but a surface that contains an inflection point, the value of which depends on the coefficients of the considered model. The response surface obtained does not differ much from the response surface from Fig. 14, which makes us infer that the coefficients associated with the interaction between the pairs of factors have values close to zero.

Fig. 16 shows the surface response for the case of the second-order approximation (Model 3). The surface obtained is similar to a parabola when both the contact stiffness axis and the clearance size axis are observed. The parabola is concave up when looking at the free space size axis, whereas it is concave down when looking at the contact stiffness axis. It can be seen that the surface has a local minimum located at a value close to 35 kN/m, while in the case of the clearance size axis, a local maximum can be observed close to 6 mm.

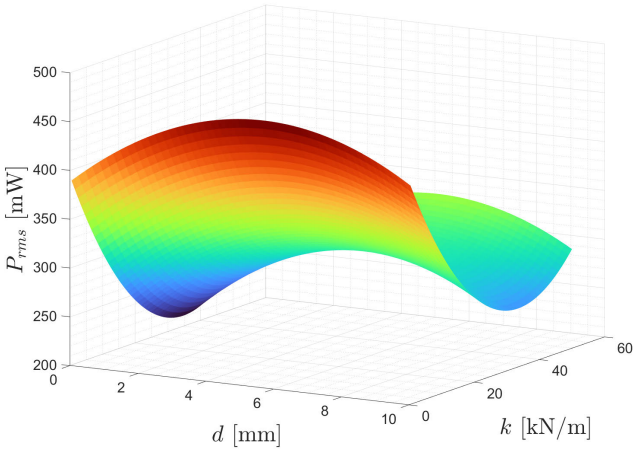

FIGURE 16. Response surface plot obtained using second-order approximation.

VI. DISCUSSION

The results presented in this study demonstrate that the presence of clearance in mechanical joints has a positive impact on energy harvesting systems. Higher power outputs have been obtained by intentionally adding larger clearance sizes, at least within the studied range of 0 to 10 mm, which corresponds to 0 to 2% of the amplitude of the assumed excitation movement.

The increase in EEHS power is explained by the presence of small vibrations superimposed on natural human movement as a result of joint clearance. The tissues of the leg and thigh, together with the mechanical elements responsible for holding the energy conversion device in the lower limb, create a vibratory system, the amplitude of which is limited by the clearance size. This phenomenon is exploited by EID, which not only recovers energy from the natural movement of the knee joint, but also recovers energy by dampening additional vibrations. In addition, it was shown that the presence of clearance in the mechanical joints significantly affects the power generated, especially when the elements that constitute the mechanical joint have little rigidity and the clearance size is relatively small. According to the results obtained, the greatest impact on P_{rms} occurs in the 1^{st} interval, that is, when a system without clearance is compared with a system with

TABLE 5. Computed coefficients for the proposed models.

Model Coefficient	Model 1	Model 2	Model 3
b_0	364.7937	370.0881	394.3027
b_1	4.5310	3.4721	29.7031
b_2	-2.6831	-2.8928	-10.5444
b_3	—	0.0419	0.0419
b_4	—	—	-2.6231
b_5	—	—	0.1515

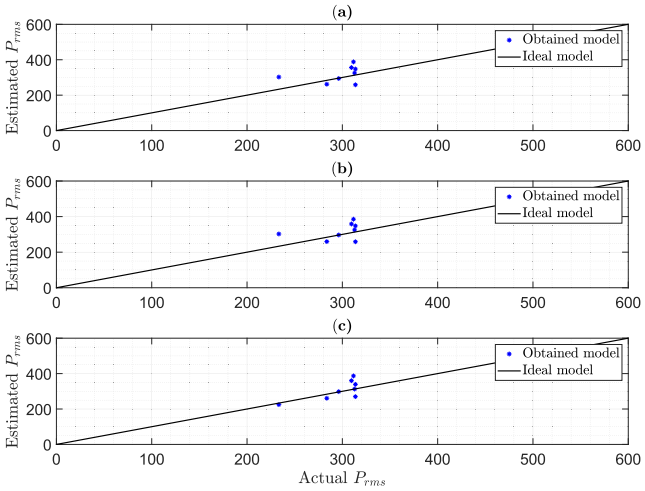

FIGURE 17. Goodness of fit. (a) Model 1. (b) Model 2. (c) Model 3.

minimal clearance, while at larger clearance sizes the increase in power is reduced.

The models obtained by using RSM allowed us to estimate the response of the EEHS when varying the factors studied, and to measure their impact on the generated power. Table 5 shows the coefficients determined for each of the proposed models. The coefficients are a measure of the impact of the studied factors on the RMS power.

Fig. 17 shows how the determined models fit the data. An ideal result is obtained when all points (represented by blue asterisks) are located on the black line. However, it should be stressed that a perfect fit of the data does not mean that the response surface geometry is correct, since high-order approximations introduce unwanted oscillations.

VII. CONCLUSION

In this investigation, a simplified model for an EEHS suitable for recovering energy from human walking has been formulated. The model differs from the others by considering the presence of joint clearance between the mechanical elements that hold the energy conversion device to the lower limb. The natural movement of the lower limb is the input for the formulated model, which considers the non-linear interaction of the electromagnetic device and the power conditioning circuit, and estimates the output voltage of the electromagnetic device.

In the course of the investigation, the differential equations that describe the dynamics of the system were determined by implementing the state-space averaging representation method. The obtained set of differential equations was solved using numerical methods, and CCD-based RSM was used to assess the impact of joint clearance size and contact stiffness on the dynamics of the system.

It was revealed that an increase of around 27% in the output power could be achieved when the joint clearance size increases, at least in the range considered (0 to 2% of the amplitude of the excitation movement). Similarly, the output power decreases when larger values of contact stiffness are considered. It was evidenced that elements with low rigidity in mechanical joints positively affect the generated power when considering small clearance sizes, while at large clearance sizes its impact is insignificant.

REFERENCES

[1] M. Liu, F. Qian, J. Mi, and L. Zuo, "Biomechanical energy harvesting for wearable and mobile devices: State-of-the-art and future directions," *Appl. Energy*, vol. 321, Sep. 2022, Art. no. 119379.

[2] M. A. Wahba, A. S. Ashour, and R. Ghannam, "Prediction of harvestable energy for self-powered wearable healthcare devices: Filling a gap," *IEEE Access*, vol. 8, pp. 170336–170354, 2020.

[3] M. A. Halim, H. Cho, M. Salauddin, and J. Y. Park, "A miniaturized electromagnetic vibration energy harvester using flux-guided magnet stacks for human-body-induced motion," *Sens. Actuators A, Phys.*, vol. 249, pp. 23–31, Oct. 2016.

[4] S.-J. Park, S. Kim, M.-L. Seol, S.-B. Jeon, I.-W. Tcho, D. Kim, and Y.-K. Choi, "A multi-directional wind based triboelectric generator with investigation of frequency effects," *Extreme Mech. Lett.*, vol. 19, pp. 46–53, Mar. 2018.

[5] Z. Yang, A. Erturk, and J. Zu, "On the efficiency of piezoelectric energy harvesters," *Extreme Mech. Lett.*, vol. 15, pp. 26–37, Sep. 2017.

[6] P. Maharjan, T. Bhatta, M. S. Rasel, M. Salauddin, M. T. Rahman, and J. Y. Park, "High-performance cycloid inspired wearable electromagnetic energy harvester for scavenging human motion energy," *Appl. Energy*, vol. 256, Dec. 2019, Art. no. 113987.

[7] M. Shepertycky and Q. Li, "Generating electricity during walking with a lower limb-driven energy harvester: Targeting a minimum user effort," *PLoS ONE*, vol. 10, no. 6, pp. 1–16, 2015.

[8] H. H.-T. Chan, F. Gao, B. L.-H. Chung, W.-H. Liao, and J. Cao, "Knee energy harvester with variable transmission to reduce the effect on the walking gait," *Smart Mater. Struct.*, vol. 30, no. 8, Jun. 2021, Art. no. 085024.

[9] R. Riemer and A. Shapiro, "Biomechanical energy harvesting from human motion: Theory, state of the art, design guidelines, and future directions," *J. NeuroEng. Rehabil.*, vol. 8, no. 1, p. 22, Dec. 2011.

[10] K. Fan, Y. Zhang, H. Liu, M. Cai, and Q. Tan, "A nonlinear two-degree-of-freedom electromagnetic energy harvester for ultra-low frequency vibrations and human body motions," *Renew. Energy*, vol. 138, pp. 292–302, Aug. 2019.

[11] M. U. Anjum, A. Fida, I. Ahmad, and A. Iftikhar, "A broadband electromagnetic type energy harvester for smart sensor devices in biomedical applications," *Sens. Actuators A, Phys.*, vol. 277, pp. 52–59, Jul. 2018.

[12] Z. Wang, X. Wu, Y. Zhang, Y. Liu, Y. Liu, W. Cao, and C. Chen, "A new portable energy harvesting device mounted on shoes: Performance and impact on wearer," *Energies*, vol. 13, no. 15, pp. 1–14, 2020.

[13] J. M. Donelan, Q. Li, V. Naing, J. A. Hoffer, D. J. Weber, and A. D. Kuo, "Biomechanical energy harvesting: Generating electricity during walking with minimal user effort," *Science*, vol. 319, no. 5864, pp. 807–810, Feb. 2008.

[14] S. H. Collins and A. D. Kuo, "Recycling energy to restore impaired ankle function during human walking," *PLoS ONE*, vol. 5, no. 2, p. e9307, Feb. 2010.

[15] Y. Liu, L. Xu, and L. Zuo, "Design, modeling, lab, and field tests of a mechanical-motion-rectifier-based energy harvester using a ball-screw mechanism," *IEEE/ASME Trans. Mechatronics*, vol. 22, no. 5, pp. 1933–1943, Oct. 2017.

[16] G. Digregorio, H. Pierre, P. Laurent, and J.-M. Redoute, "Modeling and experimental characterization of an electromagnetic energy harvester for wearable and biomedical applications," *IEEE Access*, vol. 8, pp. 175436–175447, 2020.
[17] S. M. Varedi, H. M. Daniali, M. Dardel, and A. Fathi, "Optimal dynamic design of a planar slider-crank mechanism with a joint clearance," *Mech. Mach. Theory*, vol. 86, pp. 191–200, Apr. 2015.
[18] X. Qiu, P. Gui, G. Qiao, Y. Wei, and Z. Ren, "Influence of joint clearance on the dynamic characteristics of the lunar rover deployable panels," in *Proc. IEEE Int. Conf. Robot. Biomimetics (ROBIO)*, Dec. 2016, pp. 167–172.
[19] Y. Wang and F.-M. Li, "Nonlinear dynamics modeling and analysis of two rods connected by a joint with clearance," *Appl. Math. Model.*, vol. 39, no. 9, pp. 2518–2527, May 2015.
[20] K. Lygas, P. Wolszczak, G. Litak, and P. Staczek, "Complex response of an oscillating vertical cantilever with clearance," *Meccanica*, vol. 54, nos. 11–12, pp. 1689–1702, Sep. 2019.
[21] K. Lygas, P. Wolszczak, P. Staczek, and G. Litak, "Energy harvesting from an oscillating vertical piezoelectric cantilever with clearance," in *Energy Harvesting for Wireless Sensor Networks: Technology, Components and System Design*, O. Kanoun, Ed. Berlin, Germany: De Gruyter, 2018, pp. 125–135.
[22] F. Cheng, H. Jiang, H. Lou, R. Palomera-Arias, J. J. Connor, and J. A. Ochsendorf, "Feasibility study of passive electromagnetic damping systems," *Smart Struct.*, vol. 134, pp. 109–158, Jan. 2008.
[23] B. Li, S. Quan, W. Jin, L. Han, J. Liu, and A. He, "Identification of clearance and contact stiffness in a simplified barrel-cradle structure of artillery system," *Adv. Mech. Eng.*, vol. 7, no. 2, Jan. 2015, Art. no. 745268.
[24] L. M. Arias, J. Iwaniec, and M. Iwaniec, "Modeling and analysis of the power conditioning circuit for an electromagnetic human walking-induced energy harvester," *Energies*, vol. 14, no. 12, p. 3367, Jun. 2021.
[25] P. T. Krein, B. L. C. Lesieutre, J. Bentsman, R. M. Bass, and B. L. C. Lesieutre, "On the use of averaging for the analysis of power electronic systems," *Comput. Eng.*, vol. 5, no. 1, pp. 463–467, 1989.
[26] H. A. Wheeler, "Inductance formulas for circular and square coils," *Proc. IEEE*, vol. 70, no. 12, pp. 1449–1450, Dec. 1982.
[27] U. M. Ascher and L. R. Petzold, *Computer Methods for Ordinary Differential Equations and Differential-Algebraic Equations*, 1st ed. Philadelphia, PA, USA: Society for Industrial and Applied Mathematics, 1998.
[28] E. Foray, C. Martin, B. Allard, and P. Bevilacqua, "A design-of-experiments-based approach to design planar transformers for high-voltage low-power applications," *IEEE Trans. Magn.*, vol. 58, no. 6, pp. 4–9, Jun. 2022.
[29] J. Kolb and K. Hameyer, "Sensitivity analysis of manufacturing tolerances in permanent magnet synchronous machines with stator segmentation," *IEEE Trans. Energy Convers.*, vol. 35, no. 4, pp. 2210–2221, Dec. 2020.
[30] M.-T. Duong and Y.-D. Chun, "Optimal design of a novel exterior permanent magnet tubular machine for energy harvesting from vehicle suspension system," *IEEE Trans. Energy Convers.*, vol. 35, no. 4, pp. 1772–1780, Dec. 2020.

LUDWIN MOLINA ARIAS was born in Barranquilla, Colombia, in 1994. He received the B.S. degree in mechanical engineering from Universidad del Norte, Barranquilla, in 2016, and the M.S. degree in biomedical engineering from the AGH University of Science and Technology, Kraków, Poland, in 2019, where he is currently pursuing the Ph.D. degree in mechanical engineering. His research interests include the modeling of biomechanical systems, motion analysis, and the development of energy harvesting devices.

MAREK IWANIEC was born in Kraków, Poland. He received the bachelor's, M.Sc., and Ph.D. degrees in mechanical engineering from the AGH University of Science and Technology, Kraków, in 1992, 1993, and 1998, respectively.

Since 1994, he has been with the AGH University of Science and Technology. He has enhanced his professional qualifications through research internships at various companies and universities, such as Muller GmbH Design Office, Germany; Eindhoven University of Technology, The Netherlands; Helsingin Energia, Finland; Lviv Polytechnic National University, Ukraine; and University La Sapienza, Italy. His research interests include the modeling of biomechanical systems, the design of diagnostic and rehabilitation devices, and the analysis of energy propagation in complex systems.

JOANNA IWANIEC was born in Kraków, Poland. She received the bachelor's, M.Sc., and Ph.D. degrees in mechanical engineering from the AGH University of Science and Technology, Kraków. She is currently an Academic Researcher with the AGH University of Science and Technology. She has participated in 15 research projects, of which three she was the project manager. She is the author of more than 100 scientific articles and six books. Her research interests include the development of damage detection methods in mechanical structures (manufacturing machinery, robots, and general structures), modal analysis, nonlinear dynamics, and biomechanics.